Vibrational Couplings in Hydridocarbonyl Complexes: A 2D-IR Perspective

Fernandez-Teran, Ricardo ; Ruf, Jeannette ; Hamm, Peter

Abstract: Hydridocarbonyl complexes, a class of industrially relevant catalysts, contain both the M–H and M–CO moieties. Here, using two-dimensional infrared spectroscopy, we examine the coupling of the typically weak M–H stretching mode and the intense M(C O) mode. By studying a series of Ir(I)- and Ir(III)-based hydridocarbonyl complexes, we show that the arrangement of the H and CO ligands in a trans configuration leads to strong vibrational coupling and mode delocalization. In contrast, a cis arrangement leads to no coupling, with the localized M–H mode having a much larger anharmonicity. These results highlight a promising strategy for enhancing the M–H vibration by intensity borrowing from the strong C O modes in a trans configuration, allowing for direct determination by infrared spectroscopy of both the oxidation (by frequency shifts) and the protonation state (via vibrational coupling) of the complex, in mechanistic studies of proton-coupled electron transfer reactions.

DOI: https://doi.org/10.1021/acs.inorgchem.0c00750

Vibrational couplings in hydridocarbonyl complexes: a 2D-IR perspective

Ricardo Fernández-Terán,* Jeannette Ruf, and Peter Hamm

Department of Chemistry, University of Zurich. Winterthurerstrasse 190, Zurich, Switzerland

E-mail: Ricardo.Fernandez@chem.uzh.ch

Phone: +41 44 635 44 73. Fax: +41 44 635 68 38

Abstract

Abstract: Hydridocarbonyl complexes, a class of industrially relevant catalysts, contain both the M–H and M–CO moieties. Here, by using two-dimensional infrared spectroscopy, we examine the coupling of the typically weak M–H stretching mode and the intense M(C≡O) mode. By studying a series of Ir(I) and Ir(III)-based hydridocarbonyl complexes, we show that the arrangement of the H and CO ligands in a *trans* configuration leads to strong vibrational coupling and mode delocalisation. In contrast, a *cis* arrangement leads to no coupling, with the localised M–H mode having a much larger anharmonicity. These results highlight a promising strategy for enhancing the M–H vibration by intensity borrowing from the strong C≡O modes in a *trans* configuration, allowing for direct determination by infrared spectroscopy of both the oxidation (by frequency shifts) and protonation state (via vibrational coupling) of the complex, in mechanistic studies of proton coupled electron transfer reactions.

Introduction

Transition metal hydride complexes play a central role as fundamental intermediates in many chemical transformations. Among these, proton and CO_2 reduction are the most prominent examples, for their relevance in addressing the global energy challenge through solar fuel production.[1,2]

A subset of transition metal hydrides, containing both M–H and M–CO moieties—also known as hydridocarbonyl complexes, are not only very active and industrially relevant hydroformylation catalysts (especially those of Ir and Rh),[3–5] but have also been used as mechanistic probes for proton-coupled electron transfer (PCET) reactions (mostly tungsten-based complexes). These reactions constitute fundamental steps in proton reduction and solar fuel production, among many other chemically relevant transformations.[6] In this context, it has been shown that electron transfer driving force, applied pressure, and the ligand environment can all vastly influence the PCET pathways,[7–9] illustrating the delicate interplay between such variables, and their role in steering reactivity.

Infrared (IR) spectroscopy has been the tool of choice for the study of transition metal carbonyl complexes, due to the very strong transition dipole of the C≡O stretching modes, which serve as ubiquitous probes for electronic density (i.e. oxidation state) at a transition metal centre.[5] Their characteristic absorption bands around 1900–2100 cm^{-1} (for terminal carbonyls) situates them in a nearly overlap-free and vastly solvent-transparent region. Terminal M–H stretches are one of the few modes with similar absorption frequencies (ranging from 1700–2250 cm^{-1}), and are known to have extremely variable (and typically low) extinction coefficients; the latter often precluding their study.[10]

Aspects such as couplings, exchange and orientations, not evident in an FT-IR absorption spectrum, become observable through multidimensional spectroscopic methods. For instance, two-dimensional infrared (2D-IR) spectroscopy provides insight into the coupling of different vibrational modes. By frequency resolving the pump (or excitation) axis, a series of diagonal and off-diagonal responses are obtained. A cross peak is observed when-

ever excitation of one mode influences the response of other modes, either through coupling or exchange. In addition, diagonal peaks yield information about solvation, and allow the distinction of inhomogeneous vs homogeneous broadening mechanisms.[11]

In this regard, 2D-IR spectroscopy has been used to study many aspects of metal carbonyl complexes,[12–17] as well as solvation dynamics of Vaska's complex, and its O_2 and I_2 adducts in binary solvent mixtures.[18–22] Lately, 2D-IR spectroscopy has also been used to distinguish exchanging conformations of a Rh(I) hydridocarbonyl complex.[23] A recent report from our group on the Pt–H stretching mode on a metal surface showed, by means of 2D-IR spectroscopy, that this mode can be characterised by its frequency, lifetime, and large anharmonicity: ca. 90 cm^{-1} for Pt–H vs 20–25 cm^{-1} for Pt(C≡O). At the same time, it was shown that the stretching mode of the surface-bound hydride has a comparable absorption cross section to that of the strong Pt(C≡O) mode.[24]

Considering the structural specificity and time resolution provided by IR spectroscopy, we chose to take a closer look into the ultrafast dynamics of the M–H and M(C≡O) bands of transition metal hydridocarbonyl complexes in solution. Herein, we employ 2D-IR spectroscopy to study a series of Ir-based hydridocarbonyl complexes in order to understand the vibrational couplings between the M–H and M(C≡O) modes, revealing their dependence on the relative orientation of the CO and H ligands.

Experimental

Chemicals and solvents

All reactions were performed under nitrogen atmosphere using standard Schlenk techniques. Solvents used for synthesis were of reagent grade or higher, and used as received. $[Ir(CO)Cl(PPh_3)_2]$ (Vaska's complex, **VC**; Strem Chemicals), and $[HIr(CO)(PPh_3)_3]$ (**IrHCOP$_3$**; Acros Organics) were used without further purification. Solvents for 2D-IR and FT-IR measurements were degassed (when needed) by freeze-pump-thaw cycles (3×) and handled under inert at-

mosphere. H_2 (PanGas AG, grade 6.0) as well as D_2 (PanGas AG, grade 3.0) were passed through ambient temperature point-of-use gas purifiers (MC1-904F, SAES Pure Gas), reducing the impurity levels in the gas stream to less than 1 ppb.

Synthesis of the complexes

The dihydrogen adduct of Vaska's complex, $[IrH_2(CO)Cl(PPh_3)_2]$ (**VC-H_2**) was prepared *in situ* by bubbling a solution of **VC** (ca. 10 mM in $CHCl_3$) with H_2 (or D_2 for **VC-D_2**) until the ν_{CO} band of the starting material decayed to a constant value (typically within 30 min, resulting in >90% conversion). During the measurements, an atmosphere of H_2 was maintained over the solution to avoid decomposition of the product. In a similar manner, the HCl adduct of Vaska's complex, $[IrH(CO)Cl_2(PPh_3)_2]$ (**VC-HCl**) was prepared *in situ* by adding one drop of conc. HCl (35% aq.) to a solution of **VC** (ca. 20 mM in $CHCl_3$), resulting in an discolouration after mixing, and in quantitative conversion into **VC-HCl**. Upon standing, a white precipitate was formed on a 10 min timescale. In both cases, degassing the solvent was crucial to minimise the formation of the oxygen adduct of Vaska's complex, $[Ir(\eta^2{-}O_2)(CO)Cl(PPh_3)_2]$ (**VC-O_2**).

Steady-state spectroscopic characterisation

FT-IR spectra were collected on a Bruker Vertex 80v spectrometer. The measurements were performed in a home-built flow cell consisting of two 2 mm thick CaF_2 windows separated by a 200 μm thick PTFE spacer. For the very insoluble **VC-HCl** complex, a 1 mm PTFE spacer was used instead (also for 2D-IR, see below).

Ultrafast 2D-IR spectroscopy

The ultrafast 2D-IR spectrometer used in this work is based on the output of a 5 kHz Ti:Sapphire amplifier producing ∼100 fs pulses centred at 800 nm, which was used to pump

a home-built mid-IR OPA,[25,26] delivering ∼2 μJ, ca. 120 fs pulses centred around 2000–2150 cm^{-1}, with a bandwidth of ca. 200 cm^{-1}. A small fraction of the mid-IR light was split from a BaF_2 wedge to be used as the probe and reference beams. Absorptive 2D-IR spectra were obtained by fast scanning the coherence delay (t_1) between the two collinear mid-IR pump pulses (up to 3.5 ps) generated in a Mach-Zehnder interferometer for a fixed population delay (t_2).[27] Scattering suppression was achieved by quasi-phase cycling using a librating ZnSe window introduced at Brewster angle in the pump beam.[28] The pump and probe beams were overlapped at the sample position, and afterwards the probe and reference beams were dispersed in a spectrograph with a 100 or 150 l mm^{-1} grating. Both were simultaneously recorded with a 2×32 pixels MCT array detector, yielding an ω_3 resolution of ca. 10.4 or 5.5 cm^{-1}, and an ω_1 resolution of ca. 2 cm^{-1}, respectively. In all experiments, the pump and probe beams were *p*-polarised.

Computational details

Density functional theory (DFT) calculations were performed using Gaussian 09 rev. D.01[29] with the B3LYP functional, the 6-311G(d,p) basis set for all light atoms, and the LANL2DZ effective core potential for the Ir atoms.[30–32] The IEF-PCM solvation model (as implemented in Gaussian) was used for calculations in solution.[33] Harmonic vibrational analysis revealed no negative frequencies, confirming the structures to be true minima. Anharmonic vibrational analysis were performed on the reduced subspace of the Ir–H and Ir(C≡O) normal modes. The anharmonic treatment of the vibrations was performed using the Gaussian 09 rev. D.01 implementation of the generalized second-order vibrational perturbation theory (GVPT2), including terms up to the third and fourth derivatives of the potential energy with respect to the normal mode coordinates.[34]

Results and discussion

Intermode coupling in $IrHCOP_3$

As a starting point, we turn to the absorption and 2D-IR spectra of **$IrHCOP_3$** (Figure 1). This Ir(I) complex, containing only one CO and one hydride ligand in a *trans* configuration, constitutes the simplest model system.

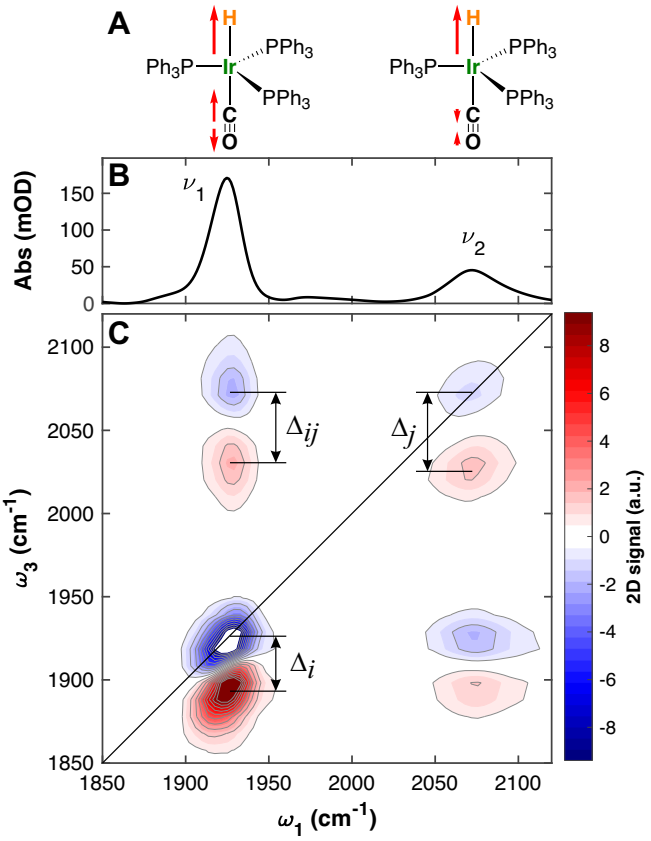

Figure 1: (A) Normal modes and scaled displacement vectors. Absorption (B) and 2D-IR spectra (C) of **$IrHCOP_3$** in DMF, with 1.5 eq. PPh_3 (at $t_2 = 3$ ps).

Its absorption spectrum in DMF shows two strong absorption bands centred around $\nu_1 = 1925$ and $\nu_2 = 2073$ cm^{-1}, corresponding to the symmetric and antisymmetric H–Ir(C≡O) stretching modes, respectively, according to the DFT calculations (Figure 1A-B). In the 2D-IR spectra, strong instantaneous cross peaks can be observed between the ν_1 and ν_2 bands, indicative of direct coupling between these modes (Figure 1C).

To begin with, the appearance of a 2D-IR spectrum relies on anharmonicity, as the 2D-IR

response of a strictly harmonic system would vanish. The anharmonic coupling between two modes can be quantified by the cross anharmonicity (Δ_{ij}), defined as:[11,35]

$$\Delta_{ij} = (\nu_i + \nu_j) - \nu_{ij}, \tag{1}$$

where ν_i is the fundamental anharmonic frequency, and ν_{ij} the anharmonic frequency of the combination band of modes i and j. The diagonal anharmonicity (Δ_i), refers to the difference between the $\nu_{1\rightarrow2}$ and the $\nu_{0\rightarrow1}$ transition energies. All these quantities can be (and have been) calculated from anharmonic vibrational calculations within Gaussian, which start from a (harmonic) normal mode calculation and treat anharmonicity perturbatively.[29]

It can be shown that the size of the cross anharmonicity (Eq. 1) tentatively reflects the degree to which the harmonic normal modes are delocalised.[11,35–37] This is since the source of anharmonicity is local—due to the very fact that the potential energy surface of a chemical bond is better described by a Morse potential rather than a parabolic (harmonic) potential. Upon normal mode transformation, which delocalises local modes in a harmonic sense, the local anharmonicity delocalises accordingly, revealing the cross terms Δ_{ij} (Eq. 1). The relationship between cross anharmonicity and degree of delocalization is not strict, since many parameters may start to play a role once anharmonicity is considered. However, we will report both cross anharmonicity and degree of delocalization for all molecular examples we consider, and we will see that they are indeed correlated to a significant extent.

That is, anharmonic vibrational calculations for **IrHCOP$_3$** in DMF revealed $\Delta_{12}^{\text{calc}} = 14$ cm^{-1}, in accordance with the result that harmonic normal modes are delocalised among the Ir–H and the –C≡O chemical bonds (see red displacement vectors in Figure 1A). The calculated diagonal anharmonicities ($\Delta_1^{\text{calc}} = 22$ cm^{-1} and $\Delta_2^{\text{calc}} = 61$ cm^{-1}) are also in good agreement with the experimentally observed results (Figure 1C; with $\Delta_1^{\text{exp}} = 22$, $\Delta_2^{\text{exp}} = 45$, and $\Delta_{12}^{\text{exp}} = 19$ cm^{-1}).

To assess the extent of localisation of normal modes, we have chosen the mass-weighted

length of the displacement vectors (a more detailed explanation is given in the SI). We found, using this approach, that for **IrHCOP$_3$** the fractional contributions of the Ir–H^{trans} and Ir(C≡O) moieties are, respectively, 19%:81% for ν_1, and 70%:30% for ν_2; meaning that the higher frequency band is more localised in the hydride, while the lower frequency band is more localised in the carbonyl moiety, also in line with the observed diagonal anharmonicities.

Intermode coupling in VC-HCl

The next complex we consider, **VC-HCl**, constitutes a counterexample to the discussion above. Addition of HCl to Vaska's complex has been shown to proceed in an analogous manner as for H_2, yielding [IrH(CO)Cl$_2$(PPh$_3$)$_2$] (**VC-HCl**).[38,39] In this case, only the *cis*-Cl$_2$ isomer of **VC-HCl** is obtained with the hydride being *cis* to the carbonyl ligand. This stereochemical assignment has been confirmed crystallographically.[40]

The Ir–H and Ir(C≡O) modes are now decoupled (see the red displacement vectors in Figure 2A), yielding an IR absorption spectrum (Figure 2B) with a strong Ir(C≡O) stretching band ($\nu_2 = 2048$ cm^{-1}), and a very weak and broad Ir–H stretching band ($\nu_2 = 2226$ cm^{-1}). In line with the discussion above, no cross peaks are observed between the Ir(C≡O) and Ir–H^{cis} modes in the 2D-IR spectrum of this complex (Figure 2C).

Anharmonic DFT calculations indeed yield $\Delta_{12}^{calc} \approx 0$ cm^{-1} for the cross anharmonicity, while the diagonal anharmonicities are once more in excellent agreement with the experiment ($\Delta_1^{calc} = 24$, and $\Delta_2^{calc} = 82$ cm^{-1}, vs $\Delta_1^{exp} = 24$ and $\Delta_2^{exp} = 71$ cm^{-1}). For this complex, the fractional contributions of the Ir–H^{cis} and Ir(C≡O) moieties are, respectively, 1%:99% for ν_1, and 100%:0% for ν_2, reflecting the totally localised characters of these vibrations.

We also see that a localised M–H vibration has a significantly larger anharmonicity (typ. > 80 cm^{-1}) , in comparison to that of the M(C≡O) modes (typ. $\sim$20 cm^{-1}). Similarly large anharmonicities are found in the O–H stretches of water,[41] phenol,[42] and other oscillators involving an H atom. In particular, the Ir–H anharmonicity in solution ($\Delta_{Ir–H} \approx 70$ cm^{-1}) compares favourably with that of Pt–H on a metal surface ($\Delta_{Pt–H} \approx 90$ cm^{-1}).[24] This can be

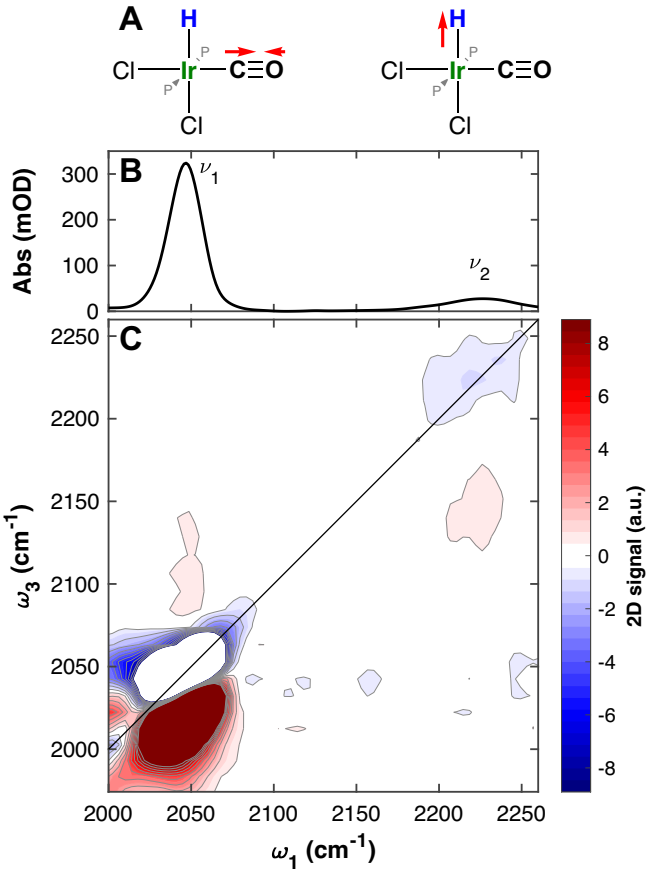

Figure 2: (*A*) Normal modes and scaled displacement vectors. Absorption (*B*) and 2D-IR spectra (*C*) of **VC-HCl** in $CHCl_3$ (at $t_2 = 3$ ps). The scale of the 2D-IR spectrum has been expanded to approx. 8% of the maximum, in order to show the very weak Ir–H band (ν_2). Phosphine ligands simplified for clarity.

explained in simple terms: the M–H fragment, having a much lower reduced mass, explores a larger extent of its potential energy surface.

Intermode coupling in VC-H_2

The final example, **VC-H_2**, combines both situations with two hydride ligands, one of which is *trans* to the CO ligand and the other *cis*. Concerted oxidative addition of H_2 to the Ir(I) centre in Vaska's complex leads to a *cis*-dihydride complex (Figure 3).[39] The two hydrides add to the metal in a mutually *cis* fashion due to homolytic cleavage of the H–H bond, effectively transforming the complex from square planar to octahedral geometry, and increasing the oxidation state of the metal to Ir(III). These changes are evident in the FT-IR

spectra of the **VC-H$_2$** complex, where the ν_{CO} band of **VC** at 1966 cm^{-1} disappears, and three new bands appear at 1998, 2098 and 2221 cm^{-1} (Figure 3B, black vs blue). Upon deuteration, the ν_{CO} band shifts to 2033 cm^{-1} without the appearance of other bands in this region (Figure 3B, red). Complete FTIR spectra for these complexes are provided in the SI (Figure S1).

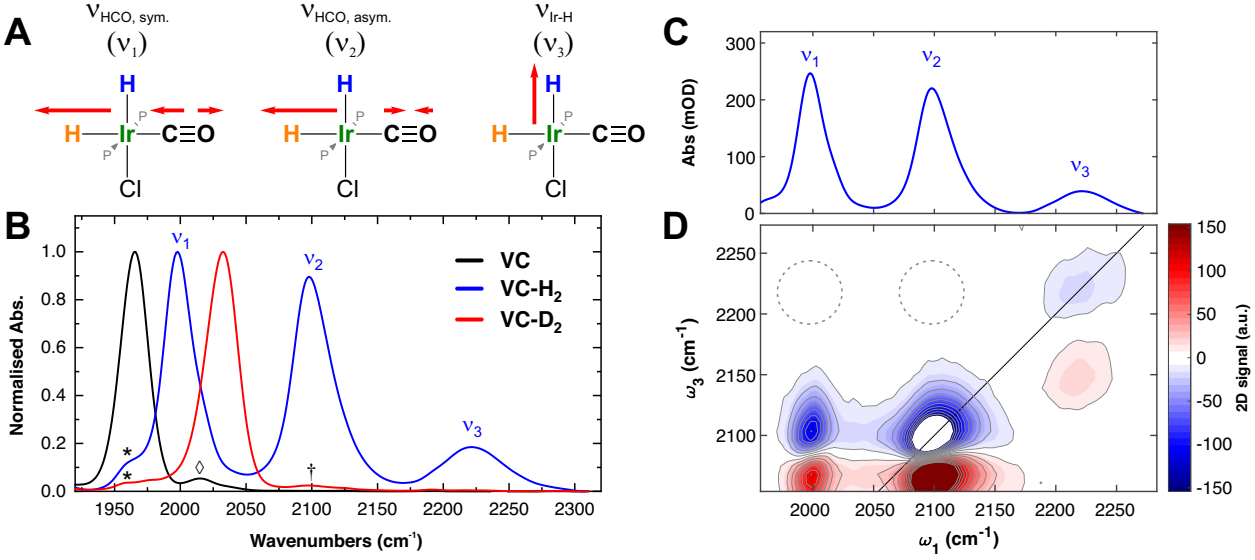

Figure 3: (*A*) Normal modes of **VC-H$_2$** with their corresponding scaled displacement vectors (phosphine ligands simplified for clarity). (*B*) Normalised absorption spectra of **VC** (*black*), **VC-H$_2$** (*blue*), and **VC-D$_2$** (*red*) in $CHCl_3$. The symbols * and ◇ in the spectra refer to traces of **VC** and **VC-O$_2$**, respectively. In the spectrum of **VC-D$_2$**, the additional, very weak bands due to partially deuterated products, or traces of **VC-H$_2$** are indicated with †. (*C*) Absorption and (*D*) 2D-IR spectra of **VC-H$_2$** in $CHCl_3$, in the 1960–2280 cm^{-1} spectral region (for *D*, $t_2 = 3$ ps). The dashed circles emphasize the missing cross peaks between ν_3 and the other modes, see text for discussion.

The corresponding 2D-IR spectrum is shown in Figure 3D, with a cross peak between ν_1 and ν_2, but none between ν_3 to any of the other two modes. Anharmonic DFT calculations for **VC-H$_2$** revealed $\Delta_{12}^{calc} = 27$ cm^{-1} (vs $\Delta_{12}^{exp} = 30$ cm^{-1}), and $\Delta_{23}^{calc} = \Delta_{13} \approx 0$ cm^{-1}, in agreement with the notion that ν_1 and ν_2 are the delocalised symmetric and antisymmetric H–Ir(C≡O) modes, while ν_3 remains a localised Ir–H mode for the *cis* hydride (see red displacement vectors in Figure 3A). The diagonal anharmonicities are also reasonably well reproduced in the DFT calculations ($\Delta_1^{calc} = 19, \Delta_2^{calc} = 54, \Delta_3^{calc} = 86$ cm^{-1}; vs $\Delta_1^{exp} = 21$,

$\Delta_2^{\text{exp}} = 26$, and $\Delta_3^{\text{exp}} = 73$ cm^{-1}).

Comparing the FT-IR spectra of **VC-H$_2$** and **VC-D$_2$**, we note that the ν_1 band of the former is closer to ν_{CO} of the latter. The magnitude of the splitting of the two modes (ca. 100 cm^{-1}) is an indicator of the coupling between them,[43,44] and can be related to the cross-anharmonicity (Δ_{12}) obtained from 2D-IR spectroscopy. This shows the potential for 2D-IR to reveal these couplings without the need for isotope labelling, showing the complementarity between both approaches.

Upon deuteration, one would expect the ν_3 band to shift to ca. 1571 cm^{-1} (based on the change of reduced mass). Indeed, we observe a weak and broad band in this region (Figure S1 in the SI), which overlaps with several other modes. We attribute this band to the Ir–D$^{\text{cis}}$ stretching mode, while the weaker bands are C=C stretching modes. The Ir–D$^{\text{trans}}$ mode becomes more difficult to locate, since it would appear in region around 1470–1500 cm^{-1}. This region is particularly crowded with C=C stretching and bending modes from the phenyl rings of the PPh_3 ligands, probably leading to mixing of the Ir–D$^{\text{trans}}$ band with the former. Our observations are in agreement with previous reports of this complex.[44] The Ir(C≡O) mode, in contrast, localises in **VC-D$_2$**. The 2D-IR spectrum in the ν_{CO} region of **VC-D$_2$** in $CHCl_3$ (Figure S2 in the SI), reveals a diagonal anharmonicity of ca. 25 cm^{-1} for this mode.

Previously, the ν_1 and ν_2 bands were assigned to the Ir(C≡O) and Ir–H stretching modes.[22,43–45] Here, it becomes clear that these bands correspond instead to the $\nu_{\text{HCO, sym.}}$ and $\nu_{\text{HCO, asym.}}$ modes, which are strongly coupled and largely delocalised.For this complex, the fractional contributions of the Ir–H$^{\text{cis}}$, Ir–H$^{\text{trans}}$, and Ir(C≡O) moieties are, respectively, 1%:25%:74% for ν_1; 3%:57%:39% for ν_2, and 95%:5%:0% for ν_3. The absence of coupling with ν_3 explains also its larger anharmonicity and lower intensity, reflecting the local character of this mode.

Two mechanisms may, in principle, lead to mode delocalisation—namely kinematic and electronic coupling. Kinematic coupling is dominant in small molecules like CO_2, and refers to the fact that the vibration of one C=O local mode affects that of the other, as they share

the same C atom (in the case of CO_2). One can easily verify that this effect is negligible here by setting the mass of the Ir atom to (effectively) infinity in the normal mode calculation, which does not result in any significant change of the calculated spectra and displacement vectors. This leaves electronic coupling of the Ir–H and Ir(C≡O) modes as the dominating effect in the present case.

Hydride ligands are among the strongest σ-donors. At the same time, bonding to carbonyl ligands has a σ and a π component (the CO ligand being a very good π-acceptor). The observed strong vibrational coupling between the M–H and M(C≡O) modes in a *trans* geometry (as well as their absence in the *cis* configuration), can be rationalised by considering the *trans*-influence of the hydride ligand—that is, electronic communication through the σ bonding orbitals of the complex allows the displacement along the M–H bond coordinate to influence the extent of backbonding on the CO ligand (and hence the C–O distance), effectively coupling the two potential energy surfaces and delocalising the vibration.[11,46,47]

It is important here to distinguish the *trans*-influence (a *thermodynamic* aspect) from the *trans*-effect (a *kinetic* aspect), especially when discussing equilibrium properties as above (in our case, electronic communication, orbital interactions, and bonding).[48,49] The *trans*-influence is maximised in octahedral d^6 complexes (like **VC-HCl** and **VC-H$_2$**) and square-planar d^8 complexes. Also, for σ-donor ligands, a trigonal bipyramidal geometry with a d^8 electronic configuration (like that of **IrHCOP$_3$**) gives rise to a strong *trans*-influence. These aspects have been previously described in ref. 50 from an orbital interaction point of view, and in ref. 43 in a more general perspective.

The coupling and mode delocalisation is different in complexes containing e.g. the *fac*-$\{Re(CO)_3\}^+$ core, where the M(C≡O) modes are strongly coupled and totally delocalised, despite the mutual *cis* arrangement of the CO ligands. In a complementary manner, this can be explained by the contribution of π back-bonding, since electronic communication takes place through the π orbitals instead.

Conclusions

In this work, we use two-dimensional infrared spectroscopy to show that the *trans* configuration of the carbonyl and hydride ligands is favourable for vibrational coupling between the M(C≡O) and M–H vibrational modes. When the two ligands are in a *cis* configuration, no vibrational coupling is observed. 2D-IR spectroscopy reveals, in this manner, the extent of coupling and delocalisation of the M–H and M(C≡O) modes, yielding complementary information as had been obtained by isotope labelling in the past. In turn, the coupling and mode delocalisation are responsible for the enhancement of the weaker M–H stretching mode. These trends were illustrated by **IrHCOP$_3$** and **VC-HCl**, having purely *trans* or *cis* H–Ir–CO configurations, respectively. In **VC-H$_2$**, having hydride ligands both *cis* and *trans* to the carbonyl ligand, strong vibrational coupling was observed exclusively with the hydride in the *trans* position. These couplings take place both in Ir(I) as well as Ir(III) complexes, highlighting the apparent independence of this effect on the oxidation state of the metal centre. We attribute the directionality of this effect to pure electronic coupling of the modes, due to communication through the σ bonding orbital joining the CO–M–H fragment. In addition, we find that the very high anharmonicity of the M–H stretches is a good indicator of the local character of these modes. Overall speaking, placing these ligands in a *trans* orientation is shown here to be beneficial to enhance the M–H stretching mode, leading to a promising strategy for the design of novel hydridocarbonyl complexes acting as PCET model systems, which allows to study the proton/hydride transfer steps directly from the metal hydride perspective using IR spectroscopy.

Associated Content

Supporting Information

The Supporting Information is available free of charge on the ACS Publications website at DOI: 10.1021/XXXXXX.

- Full FTIR spectra of **VC**, **VC-H_2** and **VC-D_2**; 2D-IR spectrum of **VC-D_2**; and a discussion concerning the use of mass-weighted displacement vectors to assess localisation of vibrational modes. (PDF)

- DFT-optimised Cartesian coordinates of **IrHCOP$_3$** in DMF; **VC-H_2** in $CHCl_3$; and **VC-HCl** in $CHCl_3$. These can be visualized with any structure viewer (e.g. Mercury). (XYZ)

Author Information

Corresponding Author:

* E-mail: Ricardo.Fernandez@chem.uzh.ch

Phone: +41 44 635 44 73; Fax: +41 44 635 68 38

ORCID identifiers

Ricardo Fernández-Terán	0000-0002-4665-3520
Jeannette Ruf	0000-0003-0495-6459
Peter Hamm	0000-0003-1106-6032

Notes

The authors declare no competing financial interest.

Acknowledgements

We thank Prof. Dr. Robin Perutz, Prof. Dr. Roger Alberto, Gökçen Tek, and Dr. Jan Helbing for insightful discussions. The work was funded by the Swiss National Science Foundation (Grant CRSII2_160801/1) and the University Research Priority Program (URPP) for Solar Light to Chemical Energy Conversion (LightChEC) of the University of Zurich.

References

(1) Gong, J.; Li, C.; Wasielewski, M. R. Advances in solar energy conversion. *Chem. Soc. Rev.* **2019**, *48*, 1862–1864.

(2) Roy, N.; Suzuki, N.; Terashima, C.; Fujishima, A. Recent improvements in the production of solar fuels: From CO 2 reduction to water splitting and artificial photosynthesis. *Bull. Chem. Soc. Jpn.* **2019**, *92*, 178–192.

(3) Evans, D.; Osborn, J. A.; Wilkinson, G. Hydroformylation of alkenes by use of rhodium complex catalysts. *J. Chem. Soc. A Inorganic, Phys. Theor.* **1968**, 3133–3142.

(4) Hartwig, J. F. *Organotransition Metal Chemistry: From Bonding to Catalysis*; University Science Books: Sausalito, California, 2010.

(5) Crabtree, R. H. *The Organometallic Chemistry of the Transition Metals*, 6th ed.; Wiley Blackwell, 2014.

(6) Adams, R. E.; Grusenmeyer, T. A.; Griffith, A. L.; Schmehl, R. H. Transition metal hydride complexes as mechanistic models for proton reduction catalysis. *Coord. Chem. Rev.* **2018**, *362*, 44–53.

(7) Bourrez, M.; Steinmetz, R.; Ott, S.; Gloaguen, F.; Hammarström, L. Concerted proton-coupled electron transfer from a metal-hydride complex. *Nat. Chem.* **2015**, *7*, 140–145.

(8) Huang, T.; Rountree, E. S.; Traywick, A. P.; Bayoumi, M.; Dempsey, J. L. Switching between Stepwise and Concerted Proton-Coupled Electron Transfer Pathways in Tungsten Hydride Activation. *J. Am. Chem. Soc.* **2018**, *140*, 14655–14669.

(9) Liu, T.; Tyburski, R.; Wang, S.; Fernández-Terán, R.; Ott, S.; Hammarström, L. Elucidating Proton-Coupled Electron Transfer Mechanisms of Metal Hydrides with Free Energy- And Pressure-Dependent Kinetics. *J. Am. Chem. Soc.* **2019**, *141*, 17245–17259.

(10) Kaesz, H. D.; Saillant, R. B. Hydride complexes of the transition metals. *Chem. Rev.* **1972**, *72*, 231–281.

(11) Hamm, P.; Zanni, M. *Concepts and methods of 2D infrared spectroscopy*; Cambridge University Press: Cambridge, 2011.

(12) Khalil, M.; Demirdöven, N.; Tokmakoff, A. Coherent 2D IR spectroscopy: Molecular structure and dynamics in solution. *J. Phys. Chem. A* **2003**, *107*, 5258–5279.

(13) Stewart, A. I.; Clark, I. P.; Towrie, M.; Ibrahim, S. K.; Parker, A. W.; Pickett, C. J.; Hunt, N. T. Structure and vibrational dynamics of model compounds of the [FeFe]-hydrogenase enzyme system via ultrafast two-dimensional infrared spectroscopy. *J. Phys. Chem. B* **2008**, *112*, 10023–10032.

(14) Baiz, C. R.; McRobbie, P. L.; Anna, J. M.; Geva, E.; Kubarych, K. J. Two-Dimensional Infrared Spectroscopy of Metal Carbonyls. *Acc. Chem. Res.* **2009**, *42*, 1395–1404.

(15) Hunt, N. T. 2D-IR spectroscopy: Ultrafast insights into biomolecule structure and function. *Chem. Soc. Rev.* **2009**, *38*, 1837–1848.

(16) Kiefer, L. M.; King, J. T.; Kubarych, K. J. Dynamics of rhenium photocatalysts revealed through ultrafast multidimensional spectroscopy. *Acc. Chem. Res.* **2015**, *48*, 1123–1130.

(17) Kiefer, L. M.; Kubarych, K. J. Two-dimensional infrared spectroscopy of coordination complexes: From solvent dynamics to photocatalysis. *Coord. Chem. Rev.* **2018**, *372*, 153–178.

(18) Jones, B. H.; Huber, C. J.; Massari, A. M. Solvation dynamics of Vaska's complex by 2D-IR spectroscopy. *J. Phys. Chem. C* **2011**, *115*, 24813–24822.

(19) Jones, B. H.; Huber, C. J.; Spector, I. C.; Tabet, A. M.; Butler, R. A. L.; Hang, Y.; Massari, A. M. Correlating solvent dynamics and chemical reaction rates using binary

solvent mixtures and two-dimensional infrared spectroscopy. *J. Chem. Phys.* **2015**, *142*, 212441.

(20) Jones, B. H.; Massari, A. M. Origins of spectral broadening in iodated Vaska's complex in binary solvent mixtures. *J. Phys. Chem. B* **2013**, *117*, 15741–15749.

(21) Jones, B. H.; Huber, C. J.; Massari, A. M. Solvent-mediated vibrational energy relaxation from Vaska's complex adducts in binary solvent mixtures. *J. Phys. Chem. A* **2013**, *117*, 6150–6157.

(22) Huber, C. J.; Anglin, T. C.; Jones, B. H.; Muthu, N.; Cramer, C. J.; Massari, A. M. Vibrational solvatochromism in Vaska's complex adducts. *J. Phys. Chem. A* **2012**, *116*, 9279–9286.

(23) Panman, M. R.; Vos, J.; Bocokić, V.; Bellini, R.; De Bruin, B.; Reek, J. H.; Woutersen, S. Exchanging conformations of a hydroformylation catalyst structurally characterized using two-dimensional vibrational spectroscopy. *Inorg. Chem.* **2013**, *52*, 14294–14298.

(24) Paleček, D.; Tek, G.; Lan, J.; Iannuzzi, M.; Hamm, P. Characterization of the Platinum-Hydrogen Bond by Surface-Sensitive Time-Resolved Infrared Spectroscopy. *J. Phys. Chem. Lett.* **2018**, *9*, 1254–1259.

(25) Hamm, P.; Lim, M.; Hochstrasser, R. M. Vibrational energy relaxation of the cyanide ion in water. *J. Chem. Phys.* **1997**, *107*, 10523–10531.

(26) Hamm, P.; Kaindl, R. A.; Stenger, J. Noise suppression in femtosecond mid-infrared light sources. *Opt. Lett.* **2000**, *25*, 1798.

(27) Helbing, J.; Hamm, P. Compact implementation of Fourier transform two-dimensional IR spectroscopy without phase ambiguity. *J. Opt. Soc. Am. B* **2011**, *28*, 171.

(28) Bloem, R.; Garrett-Roe, S.; Strzalka, H.; Hamm, P.; Donaldson, P. Enhancing signal detection and completely eliminating scattering using quasi-phase-cycling in 2D IR experiments. *Opt. Express* **2010**, *18*, 27067.

(29) Frisch, M. J. et al. Gaussian 09, Revision D.01. 2009; `http://gaussian.com/`.

(30) Hay, P. J.; Wadt, W. R. Ab initio effective core potentials for molecular calculations. Potentials for K to Au including the outermost core orbitale. *J. Chem. Phys.* **1985**, *82*, 299–310.

(31) Wadt, W. R.; Hay, P. J. Ab initio effective core potentials for molecular calculations. Potentials for main group elements Na to Bi. *J. Chem. Phys.* **1985**, *82*, 284–298.

(32) Hay, P. J.; Wadt, W. R. Ab initio effective core potentials for molecular calculations. Potentials for the transition metal atoms Sc to Hg. *J. Chem. Phys.* **1985**, *82*, 270–283.

(33) Scalmani, G.; Frisch, M. J. Continuous surface charge polarizable continuum models of solvation. I. General formalism. *J. Chem. Phys.* **2010**, *132*, 114110.

(34) Bloino, J. A VPT2 route to near-infrared spectroscopy: The role of mechanical and electrical anharmonicity. *J. Phys. Chem. A* **2015**, *119*, 5269–5287.

(35) Woutersen, S.; Hamm, P. Nonlinear two-dimensional vibrational spectroscopy of peptides. *J. Phys. Condens. Matter* **2002**, *14*, R1035.

(36) Lehmann, K. K. On the relation of Child and Lawton's harmonically coupled anharmonic-oscillator model and Darling-Dennison coupling. *J. Chem. Phys.* **1983**, *79*, 1098.

(37) Mills, I. M.; Robiette, A. G. On the relationship of normal modes to local modes in molecular vibrations. *Mol. Phys.* **1985**, *56*, 743–765.

(38) Vaska, L.; DiLuzio, J. W. Carbonyl and hydrido-carbonyl complexes of iridium by reaction with alcohols. Hydrido complexes by reaction with acid. *J. Am. Chem. Soc.* **1961**, *83*, 2784–2785.

(39) Vaska, L.; DiLuzio, J. W. Activation of Hydrogen by a Transition Metal Complex at Normal Conditions Leading to a Stable Molecular Dihydride. *J. Am. Chem. Soc.* **1962**, *84*, 679–680.

(40) Charmant, J. P.; Norman, N. C.; Orpen, A. G.; Whittell, G. R. Carbonyldichlorohydridobis(triphenyl-phosphine)iridium(III). *Acta Crystallogr. Sect. E Struct. Reports Online* **2004**, *60*, m162–m163.

(41) Perakis, F.; Marco, L. D.; Shalit, A.; Tang, F.; Kann, Z. R.; Kühne, T. D.; Torre, R.; Bonn, M.; Nagata, Y. Vibrational Spectroscopy and Dynamics of Water. *Chem. Rev.* **2016**, *116*, 7590–7607.

(42) Kwac, K.; Lee, C.; Jung, Y.; Han, J.; Kwak, K.; Zheng, J.; Fayer, M. D.; Cho, M. Phenol-benzene complexation dynamics: Quantum chemistry calculation, molecular dynamics simulations, and two dimensional IR spectroscopy. *J. Chem. Phys.* **2006**, *125*, 244508.

(43) Appleton, T. G.; Clark, H. C.; Manzer, L. E. The trans-influence: its measurement and significance. *Coord. Chem. Rev.* **1973**, *10*, 335–422.

(44) Vaska, L. Infrared Spectra and Structures of Hydridocarbonyl Complexes of Transition Metals. *J. Am. Chem. Soc.* **1966**, *88*, 4100–4101.

(45) Nakamoto, K. *Infrared and Raman Spectra of Inorganic and Coordination Compounds: Part B: Applications in Coordination, Organometallic, and Bioinorganic Chemistry*, 6th ed.; John Wiley and Sons: Hoboken, New Jersey, 2008.

(46) Miessler, G. L.; Fischer, P. J.; Tarr, D. A. *Inorganic chemistry*, 5th ed.; Pearson: Boston, 2014.

(47) Huheey, J. E.; Keiter, E. A.; Keiter, R. L. *Inorganic chemistry: principles of structure and reactivity*, 4th ed.; HarperCollins College Publishers: New York, 1993.

(48) Basolo, F.; Pearson, R. G. *Prog. Inorg. Chem. Vol. 4*; John Wiley & Sons, Ltd, 1962; pp 381–453.

(49) Pidcock, A.; Richards, R. E.; Venanzi, L. M. 195Pt-31P nuclear spin coupling constants and the nature of the trans-effect in platinum complexes. *J. Chem. Soc. A Inorganic, Phys. Theor.* **1966**, 1707–1710.

(50) Burdett, J. K.; Albright, T. A. Trans Influence and Mutual Influence of Ligands Coordinated to a Central Atom. *Inorg. Chem.* **1979**, *18*, 2112–2120.

For Table of Contents Only

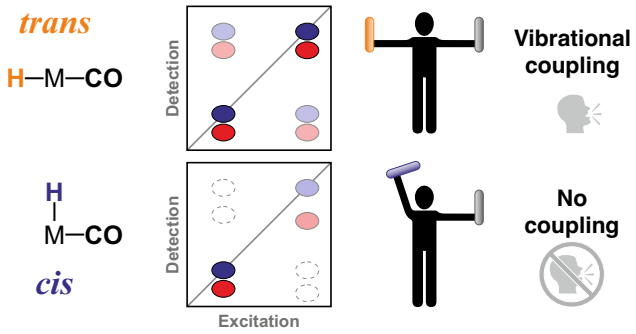

Two-dimensional infrared spectroscopy was used to reveal vibrational couplings in Ir(I) and Ir(III) hydridocarbonyl complexes in solution. The effect of the relative orientation of the carbonyl and hydride ligands was examined, revealing preferential coupling between the M–CO and M–H modes in the *trans* configuration. This approach constitutes a promising strategy to enhance the often weak M–H vibration for future mechanistic studies.